Contents lists available at ScienceDirect

European Polymer Journal

journal homepage: www.elsevier.com/locate/europolj

A novel approach for preparation of nanocomposites with an excellent rigidity/deformability balance based on reinforced HDPE with halloysite

Duarte M. Cecílio [a], Maria L. Cerrada [b,*], Ernesto Pérez [b], Auguste Fernandes [a], João Paulo Lourenço [a,c], Timothy F.L. McKenna [d], M. Rosário Ribeiro [a,*]

[a] *Centro de Química Estrutural and Departamento de Engenharia Química, Instituto Superior Técnico, Universidade de Lisboa, Av. Rovisco Pais 1, 1049-001 Lisboa, Portugal*
[b] *Instituto de Ciencia y Tecnología de Polímeros (ICTP-CSIC), Juan de la Cierva 3, 28006 Madrid, Spain*
[c] *Departamento de Química e Farmácia, Faculdade de Ciências e Tecnologia, Universidade do Algarve, Campus de Gambelas, 8005-139 Faro, Portugal*
[d] *Université de Lyon, CPE Lyon, CNRS, UMR 5128 - Catalyse, Polymérisation, Procédés et Matériaux (CP2M), Bat 308F, 43 Blvddu 11 Novembre 1918, 69616 Villeurbanne, France*

A R T I C L E   I N F O

A B S T R A C T

An innovative approach, designated as supported activator (SA), allows preparation of high density polyethylene (HDPE)-based highly performant hybrid materials. This procedure makes use of a nano-sized supported methylaluminoxane (MAO)-activator, based on halloysite natural nanotubes (HNT), combined with an *in situ* supporting concept. The new protocol when compared with a more conventional approach gives rise to higher polymerization activities as well as ultimate materials with better morphological features, greater crystallinity, thicker crystals, and highly increased stiffness. Moreover, a remarkable synergy between rigidity and toughness is attained. The Young's modulus of a film obtained from the nanocomposite with the highest HNT content increases more than 70 % relatively to a pristine HDPE film, while retaining the limit stretching ability of pristine HDPE (more than 800%). A beneficial impact of using a high aspect ratio support such as HNT in the mechanical properties is also observed, when compared to similar HDPE hybrid materials derived from dendrimer-like silica (DS) nanospheres. Interestingly, polymerization activity, polymer features and derived properties found in the ultimate materials are less impacted by support/filler nature than by preparation method. This fact highlights the crucial role of the synthetic methodology used and corroborates the high potential of the SA route for the preparation of high-performance polyethylene-based nanocomposites with an excellent balance between stiffness and deformability.

1. Introduction

Polymer-inorganic composites and, more specifically, polyolefin-inorganic ones, stand out as materials with a wide range of commercial applications. These hybrids include an organic matrix and an inorganic filler component. Combination of these two moieties usually leads to improvements in the mechanical, magnetic, or other characteristics [1–6]. The properties will vary greatly with the amount, type, and features of the inorganic loading. An important part of these materials incorporated silica as inorganic fillers [7–11]. Promising results were later obtained using nanometric fillers, to obtain the so-called nanocomposites, which leaded to greater performances than conventional composites at similar loadings. Improvements were partially ascribed to

a significant increase in the interfacial area, allowing a more suitable compatibilization at interfaces because of the nanometric size (at least in one dimension) of particles. Filler dispersion was often one of the crucial aspects in ensuring suitable ultimate performance of the nanocomposites [11–16]. Melt processing and *in-situ* polymerization [13] are the two most common methods for (nano)composites preparation. The former is more suitable for industrial production due to its much easier implementation while the latter has been proven to ensure a suitable filler dispersion in the polymeric matrix, particularly at higher loadings, turning out in superior final properties [3–6,17,18]. Moreover, further modification of the components can be performed to improve interactions at interfaces [3–6,16,19].

Halloysite natural nanotubes (HNT) can be considered as a

---

promising candidate for application in polyolefin (nano)composites. They are naturally occurring and this 1:1 layered aluminosilicate clay mineral is composed of sheets with mostly silica tetrahedra on one side, and mostly alumina octahedra on the opposite side, which causes the sheets to naturally curl into nanotubes. As such, they are similar to clays in composition, and to carbon nanotubes (CNT) in morphology [20]. Therefore, HNTs are ideal to replace the more expensive CNTs and organo-modified layersilicates in high-performance polymer nanocomposites and multi-functional nanocomposites. The characteristic length in the axial direction ranges from 200 nm to 2 µm, with an inner diameter between 10 and 40 nm and an outer diameter ranging from 40 to 70 nm [20]. Furthermore, Brunauer-Emmett-Teller (BET) surface area changes from 22.1 to 81.6 m^2/g [20].

Numerous studies have described the use of HNT as filler for polymer nanocomposites, although to the best of our knowledge, there are scarce articles on the employment of HNT as a catalyst support in olefin polymerization. Marques *et al.* [21] used vinyltrimethoxysilane (VTMS) or silicon chloride modified HNT as a support for Ziegler-Natta (Z-N) catalysts to produce high impact polypropylene (PP) composites. The authors reported a good dispersion of the HNT filler and an increase in both storage modulus and glass transition temperature when comparing the polypropylene-HNT reinforced materials with the neat polypropylene.

Development of the SA innovative methodology for the preparation of reinforced HDPE-based hybrid materials has been recently reported by the authors [22]. This approach was firstly developed employing a dendrimeric silica (DS) support and is a straightforward route that combines metallocene supporting and polymerization in a single step. The DS support is contacted with methylaluminoxane (MAO), yielding a nano-sized DS supported MAO activator, which is directly introduced into the reactor together with the homogeneous catalyst. Polymerization reaction is then undertaken by the resulting "*in situ*" supported catalyst, without the need for adding supplementary MAO. This protocol was observed to lead to a significantly higher catalytic activity regarding the one attained in systems using supported catalyst prepared by a more conventional protocol (named as DS-MAO) and similar to the activity of the corresponding homogeneous catalyst. Another important aspect is that SA protocol requires the use of a lower MAO amount than the regular procedures. The conventional DS-MAO route, on the other hand, requires a more cumbersome and time-consuming protocol comprising a two-step catalyst immobilization process onto the DS support (involving modification of the support with MAO, followed by a drying step and subsequent catalyst anchoring) as a previous stage to reactor incorporation. Then, during ethylene polymerization an additional amount of MAO is required. In terms of final characteristics, the materials prepared by the DS-SA route displayed an improved mechanical response compared with that exhibited by the DS-MAO nanocomposites, which confirmed the potential of the novel SA methodology in producing highly reinforced composite materials [23]. The improved mechanical response of DS-SA materials was ascribed to their higher crystallinity and features at the polymer-nanofiller interfaces, along with a better dispersion of the nanofiller within the HDPE matrix. Moreover, the SA method revealed a high versatility and ability in tailoring polymer properties, by changing the experimental conditions.

The aim of this article is to corroborate the potential of the SA methodology on the preparation of HDPE-based hybrids and validate its successful application using a very different support, allowing investigating the impact of support features on both polymerization behavior and properties of the final materials in an attempt of verifying the intrinsic characteristics of these two methodologies. Thus, HNT, with a high aspect ratio, was selected as either catalyst/activator carrier or filler and two sets of HNT reinforced materials were prepared, one using the novel route, designated as HNT-SA, and another employing the more conventional approach for supporting of catalysts, named as HNT-MAO. The resulting materials were characterized regarding their morphological features, filler dispersion, thermal properties (stability, crystalline

features and phase transitions) and mechanical response. A pristine HDPE specimen prepared by homogeneous polymerization using the same zirconocene catalytic system is used as a reference.

2. Experimental section

2.1. Materials

Natural HNT was kindly provided by CID Group (Mexico City, Mexico). Zirconocene dichloride (Cp_2ZrCl_2, $Cp = \eta^5\text{-}C_5H_5$, Aldrich) was used for the ethylene polymerization reactions as metallocene catalyst, and tri*iso*butylaluminum (TIBA, $[(CH_3)_2CHCH_2]_3Al$, Aldrich) was employed as a scavenger. For the preparation of the solid activator, methylaluminoxane (PMAO-IP 7 wt% in toluene, Akzo Nobel) was used as co-catalyst. Ethylene and nitrogen (Air Liquide) were purified through adsorption columns containing a mixture of 4A and 13X molecular sieves. Toluene (VWR) was dried by refluxing over metallic sodium under nitrogen and using benzophenone as an indicator. The other materials were used without further purification. All sensitive reactants and materials were handled under nitrogen using standard inert atmosphere techniques.

2.2. Support pretreatment

In this work, HNT is used as filler and support, either for the activator in the HNT-SA method, or for the catalyst in the HNT-MAO method. A batch of HNT was treated at 200 °C under primary vacuum for 90 min to remove the adsorbed water.

2.3. Composite preparation methodologies

2.3.1. HNT-SA method

500 mg of dry support were weighed and stored in a degassed Schlenk tube. Then, 10.8 g (0.117 mol) of toluene were added and vigorously stirred. MAO (0.570 g of MAO, 1.499 mmol of Al) was added to the suspension to achieve a surface Al loading of 3 mmol/g and was also vigorously stirred for 16 h at room temperature, shielded from ambient light. The HNT supported MAO suspension was then stored in a Schlenk tube until it was directly used in the polymerization reactor.

2.3.2. HNT-MAO method

The first step of this procedure was the same pretreatment just described for the HNT with MAO, albeit with an Al loading of 4 mmol/g (0.770 g of MAO, 1.998 mmol of Al). Afterwards, toluene was removed under vacuum until a light and dry powder was obtained. This dry powder was re-suspended in toluene (12.572 g, 0.136 mol) with a ratio of 29 mL per gram of support and a toluene solution (9.950 g, 0.108 mol) of zirconocene dichloride (11.75 mg, 40.2 µmol) was prepared and added to achieve a final Zr loading of 35 µmol per gram of support. After a contact time of 4 h, the final catalyst was stored in the Schlenk tube. Prior to its use in ethylene polymerization, a supernatant test is conducted to confirm complete immobilization of zirconocene dichloride on the support. To that effect, the supported catalyst suspension is left to rest until the entirety of the solid is deposited on the bottom, leaving a clear supernatant liquid on the top. Then, 1 mL of this clear liquid is introduced in the polymerization reactor where an adequate amount of MAO (same as used for the polymerization run) is already present and a polymerization run is conducted for 30 min. No polymer formation is observed, thus confirming zirconocene dichloride is not present in the supernatant and consequently that the immobilization of the catalyst on the surface of the support was complete.

2.4. Ethylene polymerization

The polymerization reactor consisted of a 250 mL bottle for pressure reactions (Wilmad LabGlass LG-3921), with crown cap, gasket, and

magnetic stirrer, and it was placed in a water bath to control polymerization temperature. Ethylene consumption rate was measured using two mass flow controllers (Hastings Instruments HFC-202 and Alicat Scientific 16 Series) and recorded in a personal computer with data acquisition hardware and software (a ComputerBoards CIO-DAS08/Jr-A0 interface card with Labtech DataLab software). Ethylene pressure was measured with a digital manometer (AirLiquide M2500) and it was also recorded.

Reactor was purged with vacuum/N_2 and loaded with enough toluene to match a total volume of 50 mL when the polymerization was started. Nitrogen was then replaced with ethylene by means of 5 vacuum/ethylene cycles and afterwards waiting for the ethylene consumption to stabilize. At this point, the procedure changes according to the preparation method employed to achieve the catalytic system.

In the case of the HNT-SA method, there is an initial addition of 1.0 mL of a 0.1 M TIBA solution to act as scavenger, followed by the addition of the appropriate volume of HNT supported MAO activator (2.9 mL per 100 mg of HNT), and finally the addition of a Cp_2ZrCl_2 toluene solution (2.0 mL) corresponding to 1.9×10^{-6} mol of Zr. No external MAO solution is added in this procedure.

The HNT-MAO method consisted in the addition of the appropriate amount of external MAO solution (2.03 g of MAO per 100 g of HNT supported catalyst, 5.259 mmol Al) to achieve an Al/Zr ratio of 1500 in the polymerization medium, followed by the addition of a vigorously stirred suspension containing the zirconocene catalyst supported onto MAO pretreated HNT, in order to achieve the desired support amount. This Al/Zr ratio was chosen to facilitate comparison with previous results using DS as support [22,23].

Polymerizations took place at 25 °C and 1.1 bar of ethylene. During the reaction the temperature, pressure and ethylene mass flow data were monitored in real-time and automatically recorded. The ethylene mass flow was converted to ethylene consumption, and polymerization activity calculated in $kg_{PE}/mol_{Zr}h$. The kinetic profiles correspond to ethylene consumption versus time, which after integration yielded a value of average activity that was compared to the value obtained by considering the mass of recovered polymer. The reaction was stopped either at the end of 30 min or when the consumption of ethylene reaches approximately 2 g, in order to avoid severe mass transfer limitations occurring after that point. After the reaction, polymer is precipitated over 5 % HCl acidified methanol (30 mL), filtered and washed twice using methanol before drying. The supernatant or clarified liquid test was followed as previously described for the HNT-MAO method, in order to assess whether the catalyst was totally immobilized on the support surface.

2.5. Film preparation

Powders obtained from these ethylene polymerizations were processed into thick films (of around 200 μm) by compression molding, using a Collin press. First of all, powders were heated up to 170 °C for 2 min without applying compression in order to properly melt the polymeric material. This stage was followed by 3 min with a pressure of approximately 2 MPa and, then, the hot compressed mass was cooled down to room temperature for 3 min in contact with metal plates refrigerated with circulating cold water, under the same pressure of 2 MPa.

2.6. Polymer molar mass characterization

Polymer average molar mass and dispersity were determined by high temperature size exclusion chromatography (HT-*SEC*) measurements, employing a Malvern Instruments Viscotek system outfitted with three Polefin 300 mm × 8 mm I.D. columns from Polymer Standards Service with corresponding porosities of 100 Å, 100,000 Å and 1,000,000 Å. 1,2,4-trichlorobenzene (TCB) was used as eluent at a 1 mL/min flow rate and a temperature of 150 °C. 2,6-di(*tert*-butyl)-4-methylphenol was used

as eluent stabilizer under a 200 mg/L concentration. The polymers were dissolved in TCB at an approximate concentration of 1 mg/mL and 200 μL injections were performed. Online detection was provided by means of a differential refractive index detector, a viscosity detector and a dual light scattering detector (right angle and low angle light scattering, RALS and LALS) for accurate measurements. OmniSEC version 5.12 was used to calculate the polymer weight parameters.

2.7. Morphological characterization

Scanning electron microscopy (SEM) micrographs were obtained on a Zeiss Merlin Compact equipment coupled with an Oxford energy-dispersive X-ray (EDX) detector. Polymer films prepared from ethylene polymerization were fixed onto the sample holder and subjected to a carbon coating procedure prior to inserting the samples into the microscope to analyze their morphological characteristics.

2.8. Nitrogen sorption isotherm

Textural properties were obtained using nitrogen sorption measurements at − 196 °C using a Micromeritics ASAP 2010 equipment. Prior to the measurements, samples were degassed, first at 100 °C for 1 h and then at 300 °C for 3 h.

2.9. Fourier transform infrared (FT-IR) measurements

Brønsted and Lewis acid site quantification was carried out through FT-IR spectroscopy with pyridine as a probe molecule. Self-supported wafers were placed in an IR quartz cell and evacuated under secondary vacuum (10^{-6} Torr) at 450 °C for 2 h before pyridine adsorption at 150 °C (equilibrium pressure ∼ 1.5 Torr). Subsequent desorption of pyridine was carried out under secondary vacuum at 150 and 350 °C for 30 min. The FT-IR spectra were recorded on a Thermo Nicolet Nexus 670 instrument (64 scans, 4 cm^{-1} resolution). The background spectrum, recorded under identical operating conditions, was automatically subtracted from each sample spectrum. For quantitative measurements, surface areas of bands at 1545 (pyridine interacting with Brønsted acid sites) and 1455 cm^{-1} (pyridine interacting with Lewis acid sites) were determined and, by using pyridine extinction molar coefficients from Emeis [24], the final amount of each acid site was calculated.

2.10. Thermal stability

Thermogravimetric analysis (TGA) was performed in a Q500 model TA instruments thermobalance under oxidative (air) and inert (nitrogen) atmospheres. Experiments were performed from 50 to 800 °C at a heating rate of 10 °C/min. These measurements allow evaluating differences in the degradation processes and assessing the actual amount of inorganic filler in the final nanocomposites.

2.11. Structural characterization

Wide angle X-ray Diffraction (WAXD) patterns were recorded at room temperature in the reflection mode to examine the crystalline structure of the polymeric materials by using a Bruker D8 Advance diffractometer provided with a PSD Vantec detector (from Bruker, Madison, Wisconsin). Cu Kα radiation ($\lambda = 0.15418$ nm) was used, operating at 40 kV and 40 mA. The parallel beam optics was adjusted by a parabolic Göbel mirror with horizontal grazing incidence Soller slit of 0.12° and LiF monochromator. The equipment was calibrated with different standards. A step scanning mode was employed for the detector. The diffraction scans were collected with a 2θ step of 0.024° and 0.2 s per step.

2.12. Phase transitions

Analyses were carried out by differential scanning calorimetry (DSC) in a TA Instruments Q100 calorimeter connected to a cooling system. Sample weights ranged from 5 to 7.5 mg. A temperature interval from −40 °C to 160 °C was chosen and a 10 °C/min running rate was employed. A 290 J/g value was used for the enthalpy of fusion of a perfectly crystalline PE [25,26].

2.13. Mechanical behavior

Nominal stress–strain (σ-ε) tests were performed at a temperature of 25 °C and a stretching rate of 10 mm/min in an MTS Q-Test Elite dynamometer with a load-cell of 100 N. Strips for these experiments were punched out from the polymer films. Dimensions of these strips were 10 mm long, 1.9 mm wide and around 0.20 mm thick. At least, three different strips were stretched until fracture for a given specimen to assess the measurement accuracy of the different parameters.

3. Results and discussion

3.1. HNT characterization

The HNT batch employed in the double role of catalyst/activator support and filler in the polymer nanocomposites was first characterized. Morphology of the particles was observed by SEM microscopy and the chemical composition was analyzed by EDX spectroscopy, as shown in Fig. 1a and Figure S1. Results confirm a needle-like particle shape, which is consistent with the nanotube shape reported previously in literature [27], with a particle length of varying size but higher than 600 nm. The EDX quantification corroborates a Si/Al ratio of 1, widely described in the existing literature.

Nitrogen sorption isotherm for the HNT batch is represented in Fig. 1b. Results suggest a type II isotherm, with a H3 hysteresis, as per International Union of Pure and Applied Chemistry (IUPAC) nomenclature [28,29]. Application of the BET theory yielded a surface area value of 32 m^2/g and a total pore volume of 0.14 cm^3/g at a relative pressure of 0.99. Further application of the BJH method yielded an average pore diameter of 17.3 nm. All values are coherent with numerous literature reports and well within the reported range [27,30,31].

Surface acidity quantification was also performed by FT-IR spectroscopy with pyridine as probe molecule. The results are summarized in Table 1. A modest acid site concentration with barely any Brønsted

Table 1

Surface acidity quantification results for the HNT batch.

Temperature (°C)	Lewis acid site concentration (μmol/g)	Brønsted acid site concentration (μmol/g)
150	22	5
350	6	1

acidity was detected. Additionally, most acidity is weak in nature, as the amount of pyridine detected at temperatures higher than 150 °C decreases markedly.

The amount of acid sites present in these HNT is much lower than those found in a synthesized batch of dendrimeric silica (DS) nanoparticles containing aluminum (Al) (DSAl materials), although in the present case a higher amount of Al compared with Si was found [32]. A similar acidity site concentration for halloysite was reported by Sidorenko *et al.* [33] with a acid site concentration of 34 μmol/g, and a predominance of Lewis acid sites present.

3.2. Preparation of the HDPE-HNT nanocomposites

In-situ polymerization is considered an appropriate route to obtain PE based nanocomposites with a fine filler dispersion, especially at high filler contents, when compared with those more commonly used melt compounding or solution mixing approaches [34]. However, different *in-situ* methodologies may present varying degrees of efficacy in terms of catalytic activity, material homogeneity, filler dispersion and amount of particle agglomerates.

Comparison in polymerization behavior between the MAO and SA methods has been reported in our previous publication [22] for incorporation of DS nanoparticles into polyethylene. In an attempt of verifying the intrinsic characteristics of these two methodologies, the synthesis of HDPE-HNT nanocomposites was performed, being labeled the procedures as HNT-SA and HNT-MAO. The polymerization time and the HNT amount incorporated were carefully controlled to produce HDPE-HNT materials with different contents in filler, from 5 to circa 20 wt%. Modification of HNT with MAO used in both methodologies exhibits the combined advantage of chemically passivating the HNT surface while creating a compatible framework whereupon the polymer can be developed.

Table 2 details the data regarding polymerization conditions, activity, HNT filler content, weight average molar mass (M_w) and dispersity (M_w/M_n) for all HNT synthesized nanocomposites, as well as for the reference HDPE attained under homogeneous conditions, while the respective kinetic profiles are shown in Figure S2 of Supporting

(a)   b)
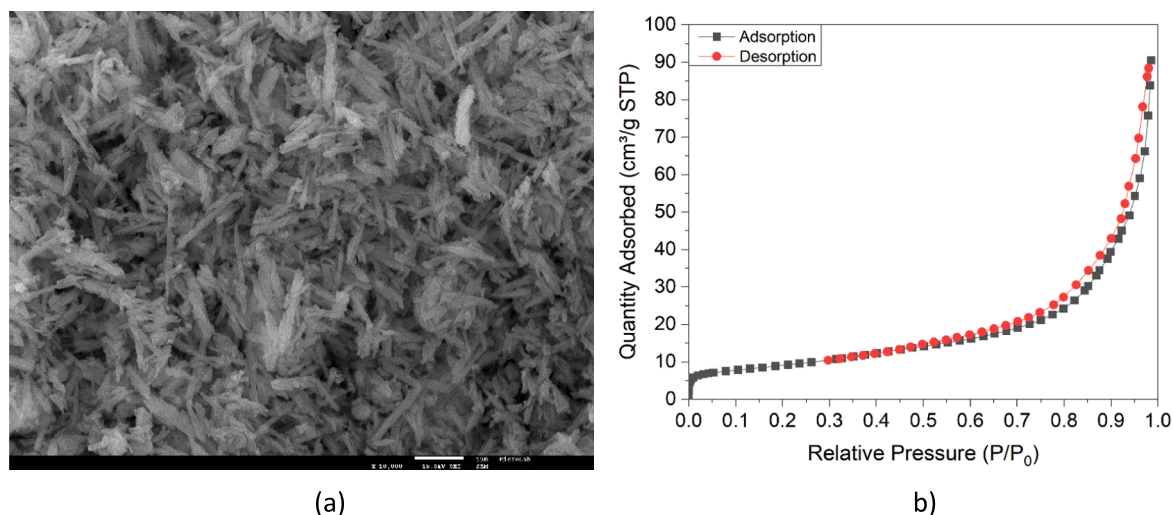
Fig. 1. (a) SEM micrograph; (b) Nitrogen sorption isotherm acquired on the HNT batch.

Table 2
Polymerization conditions and activities for the synthesis of the HDPE-HNT nanocomposites.

Sample	Support amount (mg)	Zr (μmol)	Al/Zr	Activity (kg$_{PE}$/mol$_{Zr}$h)[a]	HNT content (wt. %)[b]	M$_w$ (Da)	M$_w$/M$_n$
HDPE	–	1.9	1500	7070[c]	0	225 000	2.1
HNT-MAO-N5	50	1.8	≈ 1600	1960	5	618 000	2.2
HNT-MAO-N8	100	3.5		2240	8	461 000	1.8
HNT-MAO-N15	200	7.0		2020	15	213 000	2.2
HNT-MAO-N23	300	10.5		1450	23	184 000	2.1
HNT-SA-N5	50	1.9	110 (max)	2480	5	410 000	2.5
HNT-SA-N9	100		210 (max)	4820	9	345 000	2.5
HNT-SA-N16	200		420 (max)	8890	16	235 000	2.1
HNT-SA-N20	300		630 (max)	10,360	20	214 000	2.0

Al loading on the support = 4 and 3 mmol/g for HNT-MAO and HNT-SA methods, respectively.

[a] Presented for final polymerization time. [b]Determined by TGA. [c]Presented for 5 min.

Information. These results show that polymerization activity is strongly affected by the preparation methodology employed, leading the HNT-SA procedure to high activity values at quite low MAO amounts. At the lowest Al/Zr ratio of 110, the activity is comparable with the values obtained for the HNT-MAO procedure (at a constant Al/Zr ratio of 1600) while activities similar or even higher than those observed for the reference neat HDPE polymerization, promoted by the homogeneous catalyst, can be attained at moderate Al/Zr ratios (420 and 630).

It is important to highlight that, in both procedures, the amount of support introduced in the reactor varies equally inside the same range but, due to the specificities of each method, HNT-MAO samples are obtained at a constant Al/Zr ratio of circa 1600, while in the case of the HNT-SA specimens, the Al/Zr ratio varies significantly. Accordingly, the activities observed in the former are similar in magnitude, except for the highest support amounts wherein the high amounts of zirconocene present inside the reaction medium may lead to external diffusion limitations and to the observed loss of activity. On the other hand, the strong variation in polymerization activity for the SA procedure is ascribed to the different Al/Zr ratios used. Furthermore, the observed polymerization rate increases with the Al/Zr ratio, as expected.

The results in terms of average polymerization activity show a significant difference between the two procedures across the entire range of support/filler amount added into the reaction medium, similarly to what was observed when DS nanoparticles were used, as described in a previous work [22]. Nevertheless, the activities presented for the HNT materials are slightly lower than those exhibited previously by the DS hybrids, albeit in the same order of magnitude. The significant difference in terms of surface area and pore volume may yield – for the same MAO loading – very different concentrations of Al at the support surface, and thus, may contribute to differences in activity between the two supports. According to Chu *et al.* [35,36], it is likely that the effect of the surface area of the support on the polymerization activity becomes more noticeable in the *in-situ* supporting method in comparison with the traditional techniques. It is proposed that reduction of contact time during catalyst impregnation in this method amplifies the importance of the probability of the contact between the catalyst precursors and the potential external impregnation sites.

Concerning the HDPE molar masses, the results reported in Table 2 are within the range reported for metallocene catalyzed PEs. At low support amount / filler contents, the weight average molar mass (M_w) values obtained with both methodologies for the nanocomposites are higher than that for the homogenous HDPE used as reference, in accordance with the trend usually observed for supported catalytic systems. However, a further increase of the support amount is accompanied by a decrease in average molar mass to values closer to that exhibited by the reference HDPE. Independently of the methodology, the incorporation of higher support amounts in the reaction medium results in a larger amount of Al, which comes from MAO, that increases the probability of chain transfer to the aluminum and gives rise to shorter chains at the end of polymerizations [23].

It is also worth noting that materials prepared with the HNT-MAO procedure show higher M_w values than those achieved through the SA procedure, especially when low filler contents are considered. This trend was also observed in our previous work where these two methodologies were applied to a different support, DS. It was proposed that the inherent features to the SA procedure may result in active species that are somewhat weakly bound to the support surface and thus, the support steric protection effect, preventing β-hydride transfer, might be not as effective as for the DS-MAO procedure [23].

Overall, polymerization activity seems more dependent on the synthetic methodology (-SA or -MAO routes) than on the support used (DS or HNT). In fact, the different trends observed for the two methodologies when applied to the DS support are now corroborated by the results obtained with HNT. This highlights the specificity and distinct features of each approach and confirms the unique behavior of the SA route both in terms of catalytic activity and polymer morphology.

3.2.1. Nascent polymer morphology

Fig. 2 shows the morphology of the nascent polymeric powders obtained from extremely short polymerization runs, conducted for 30 s. A noticeable differentiation is found between the two synthetic routes. The HNT-MAO sample shows a more fibrous morphology with a large, somewhat, continuous surface made up of polymer with some visible HNT nanotubes protruding from the surface. On the other hand, the HNT-SA specimen displays a combination of spherical and polyhedral morphology with some nanotubes present as well. Similar morphological characteristics were already observed in the nanocomposites prepared from dendrimeric silica as filler/catalyst support [23], in spite of differences between the aspect ratio of DS silica and HNT.

3.2.2. Dispersion of the HNT nanotubes

Final performance of nanocomposites is strongly dependent on the filler distribution within the polymeric matrix [23]. A good dispersion maximizes the contact area between the two moieties and the reinforcing potential is enlarged if a suitable particle aggregation is prevented. At high filler contents, filler aggregation is promoted due to the different chemical nature of both components, resulting in large particle clusters that frequently lead to the reduction of the mechanical response of the composite [37]. Figures S3 and S4 of Supporting Information show SEM micrographs at distinct magnifications, comparing the filler dispersion of samples with different filler weight contents.

The results show clear differences at low filler content between the preparation methods, as deduced when comparing the composite HNT-MAO-8 with the HNT-SA-N9 one. The SA protocol leads to much better filler dispersion in the HDPE matrix compared with that observed with the MAO preparation route, (sample HNT-MAO-N8), which displays different regions: darker zones consisting mostly of polymer and lighter ones composed by aggregates of filler particles. Nevertheless, this difference is less evident in the nanocomposites HNT-MAO-N23 and HNT-SA-N20.
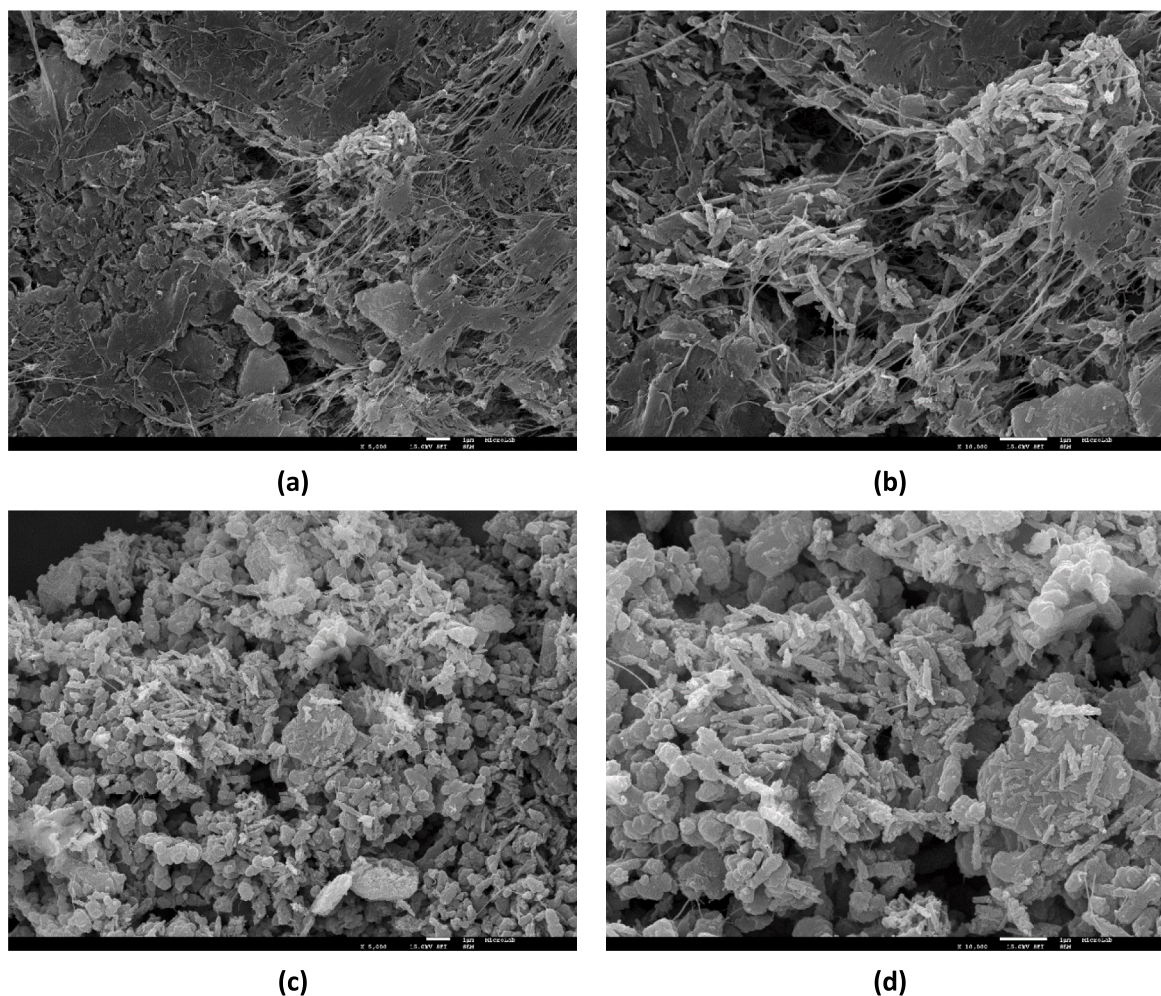
Fig. 2. SEM micrographs of polyethylene particles produced via the HNT-MAO (a, b) and HNT-SA (c, d) methods with different magnifications: 5000 times (left) and 10,000 times (right).

Additionally, all HNT nanocomposites show large white particles, regardless of filler content or preparation method. Halloysite nanotubes are natural (not synthetic) fillers and then, when they are collected, a small amount of other types of aluminosilicates can be present, like kaolinite. As such, the larger particles observed may be in fact particles of different mineral clay. This can affect somehow final characteristics of nanocomposites although the influence will be analogous in both families synthesized by the two protocols since the HNT nanotubes used are the same.

Fig. 3 shows the SEM-EDX micrographs highlighting the dispersion of the filler through a cross-section of the cryo-fractured composite films while Figure S5 of Supporting Information displays images generated from superimposed elemental mapping performed on the images represented in Fig. 3.

Results deduced from Fig. 3 and Figure S5 corroborate those achieved from Figure S3 and Figure S4. Dispersion of the fillers is more homogeneous in the HNT-SA nanocomposites than in the HNT-MAO hybrids. Samples prepared by the latter method exhibit well differentiated areas with mainly carbon (in red, Figure S5) and others with mainly silicon (in yellow) regardless of the filler content, while those prepared by the former present a much more uniform distribution. Moreover, the elemental mapping performed on the larger particles seen in the different micrographs, but especially present in sample HNT-MAO-N23, show a similar composition for the more abundant nanotubes, supporting the hypothesis that the particles are indeed other natural clays of different morphology mixed with the HNT nanotubes.

According to the results just discussed, differences in the dispersion of the HNT filler within the HDPE matrix have been found in such a way that HNT-SA family presents a better HNT dispersion than the HNT-MAO set of nanocomposites. A similar trend was observed for HDPE nanocomposites derived from incorporation of DS silica through the DS-SA and DS-MAO methodologies [23].

3.2.3. Thermal stability of the nanocomposites

The following characterization of the composite materials consisted in the study of the thermal stability, by TGA. Presence of inorganic (nano)particles, such as mesoporous silica, has been sometimes linked to a certain degree of catalytic effect in the thermal degradation of the polymers where they were incorporated [9,36,38]. The thermogravimetric curves for all the composite samples, as well as for the reference pristine HDPE, are shown in Fig. 4. Furthermore, Table 3 presents the decomposition temperatures at 5, 20 and 50 % weight loss under both, oxidative and inert, atmospheres for the different nanocomposites and for the neat HDPE.

Results represented in Fig. 4 and listed in Table 3 show that HDPE decomposition under inert conditions takes place in a single step, while several processes can be observed under oxidative atmosphere in the different thermogravimetric curves.

The loss of 5 % weight of HDPE, see values of $T_{5\%}$ in Table 3, under oxidative atmosphere indicates that the presence of clay particles inside the matrix has a stabilizing effect in the decomposition process, effectively slowing its rate until the main decomposition process starts.
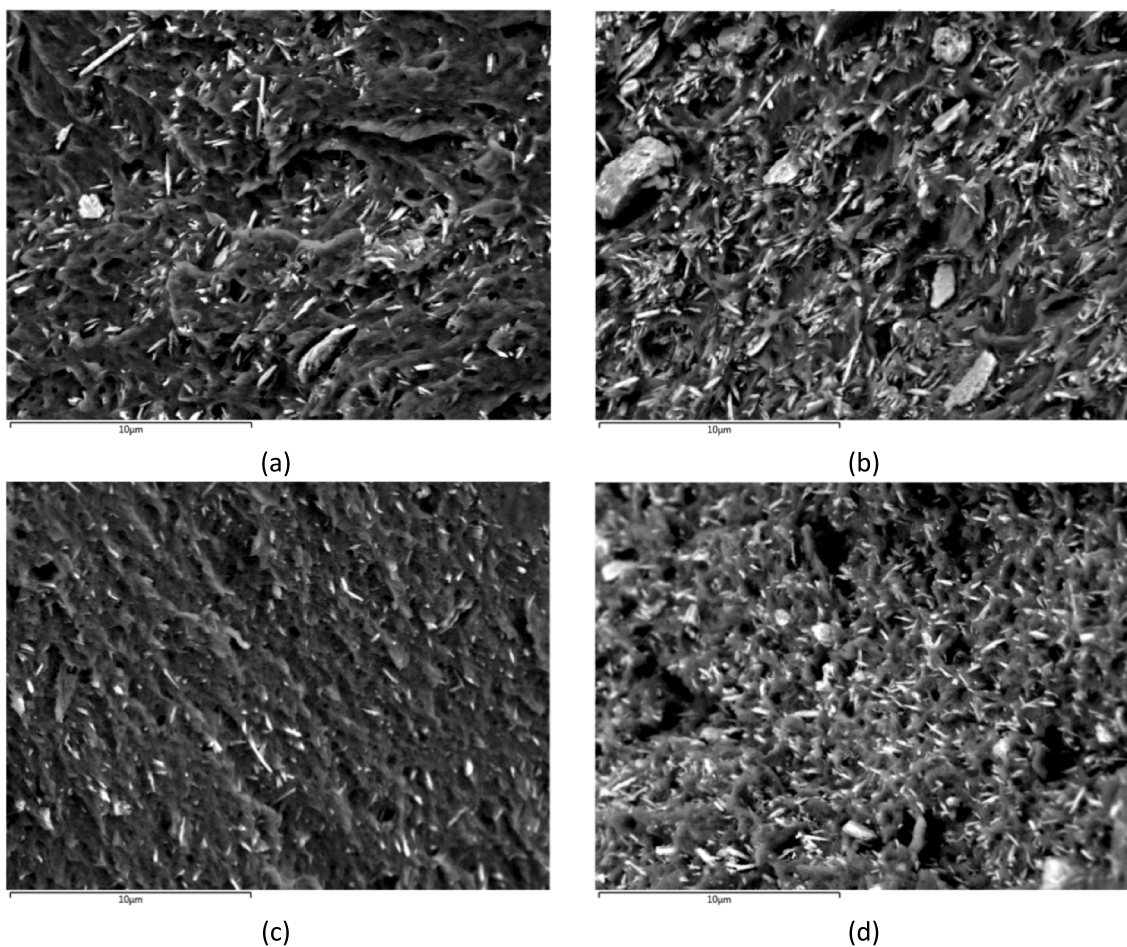
Fig. 3. SEM-EDX micrographs at 5000 times magnification of samples: HNT-MAO-N8 (a), HNT-MAO-N23 (b), HNT-SA-N9 (c) and HNT-SA-N20 (d), highlighting the dispersion of filler along the cross-section of the composite film.
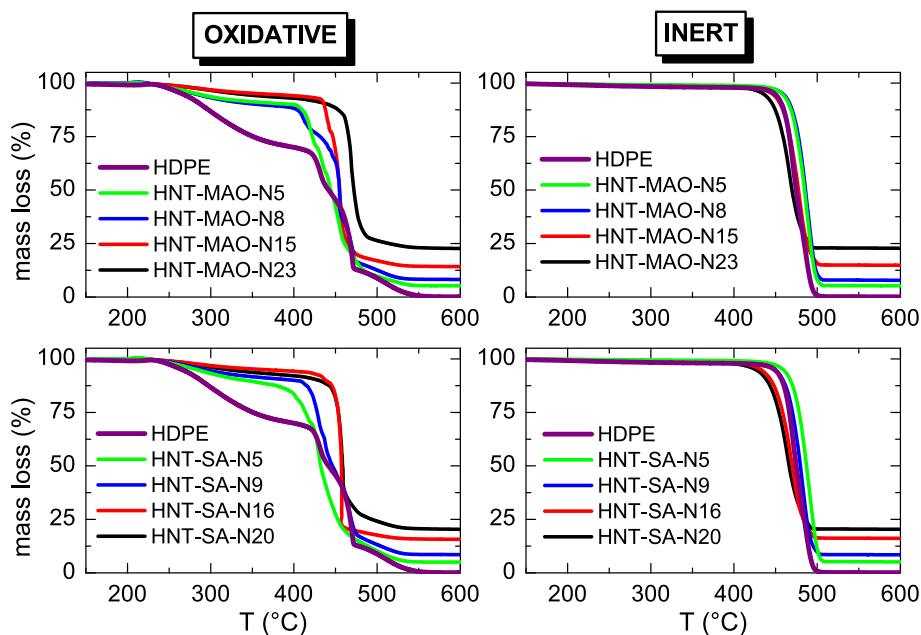

Fig. 4. Weight loss curves obtained from TGA for the HDPE/HNT nanocomposites under oxidative (left plots) and inert (right plots) atmospheres. HDPE is added as a reference for comparison.

Table 3

Thermogravimetric analysis results of the prepared nanocomposites and reference pristine polyethylene; bulk HNT filler content and decomposition temperatures at specific weight loss values of 5%, 20% and 50% under inert and oxidative atmospheres.

Sample	HNT content (wt%)[a]	Oxidative atmosphere			Inert atmosphere		
		$T_{5\%}$ (°C)	$T_{20\%}$ (°C)	$T_{50\%}$ (°C)	$T_{5\%}$ (°C)	$T_{20\%}$ (°C)	$T_{50\%}$ (°C)
HDPE	0	267	330	445	450	465	475
HNT-MAO-N5	5	284	419	444	458	473	485
HNT-MAO-N8	8	281	416	455	459	475	486
HNT-MAO-N15	15	361	442	455	446	464	477
HNT-MAO-N23	23	332	463	472	435	456	470
HNT-SA-N5	5	283	407	432	459	476	487
HNT-SA-N9	9	293	425	446	449	468	480
HNT-SA-N16	16	364	451	457	432	455	470
HNT-SA-N20	20	320	451	458	426	450	466

[a] Averaged between the weight content estimated in oxidative and inert atmospheres.

Stabilizing and flame retardant effects have been described in the literature for HNT materials, particularly when applied as fillers in composites [20,27,34,39]. A trend can be found considering the beginning of the decomposition process ($T_{5\%}$ and $T_{20\%}$), where a bigger retardant effect to decomposition is attained as filler content increases. Comparison of nanocomposites prepared by both protocols, the HNT-MAO and HNT-SA procedures, leads the conclusion that no important differences are seen between the two families of materials. In fact, an important increase in the $T_{5\%}$ is noticed in HNT-MAO-N15 and in HNT-SA-N16 nanocomposites and a later decrease at the highest HNT composition in both sets. Formation of more aggregates as HNT content increases might cause this relative temperature reduction in $T_{5\%}$, although the value is much greater than that exhibited by HDPE.

When inert experiments are examined, no clear trend is observed. At lower filler contents, decomposition temperature at 50 % weight loss ($T_{50\%}$) is slightly superior in the nanocomposites than in the neat HDPE, independently of the synthetic approach used during their preparation. Nevertheless, that temperature is a little reduced at the highest HNT loadings. It is worth noting that while analyzing these effects, the filler content varies simultaneously with the molar mass of the HDPE matrix, which may also influence the decomposition temperature.

3.2.4. Crystalline structure and phase transitions of the nanocomposites

Overall, crystalline features (type of crystalline lattice, degree of crystallinity, melting and crystallization temperatures, among others) are also critical aspects in the ultimate performance of the resulting materials. Figure S6 in Supporting Information displays the diffraction profiles at wide angles (WAXD) and at room temperature for the different HDPE nanocomposites reinforced with HNT. The pattern of the neat HDPE (polymerized under homogeneous conditions) is also included. Polyethylene crystallizes commonly in an orthorhombic lattice [40,41], being noticeable from Figure S6 that all the materials analyzed have developed that crystalline polymorph, characterized by the main reflections [42,43] (1 1 0) and (2 0 0). Presence of HNT does not affect the ordering capacity exhibited by the HDPE matrix.

Crystallinity (f_c^{WAXD}) can be determined from those WAXD diffractograms, via a deconvolution approach into the crystalline diffractions and the amorphous halo. The results are listed in Table 4. There are no differences between the values found for these two sets of nanocomposites. This constancy is also deduced from the location of the two main diffractions in the distinct samples compared with that in the pristine HDPE, as noted in Figure S6 Thus, the incorporation of HNT does not affect the spacings of the crystal lattice.

Fig. 5 exhibits the DSC curves corresponding to the first heating and subsequent cooling run for the different HNT nanocomposites. Two dissimilar tendencies are observed in the melting temperatures (T_m) when compared with that found for the neat HDPE. On one hand, a decreasing trend is seen with increasing content in HNT for the HNT-MAO hybrids, apart from sample HNT-MAO-N8. Thus, sample HNT-MAO-N23 shows a T_m value approximately 5 °C lower than that observed for the neat HDPE, as listed in Table 4, which is indicative of the existence of smaller crystallites in the former. It is true, however, that the molecular weight of HDPE is higher than that for HNT-MAO-N23 (see Table 2). Nevertheless, a difference of 3 °C is also observed for HNT-MAO-N15, with a molecular weight similar to that of HDPE. On the other hand, T_m location is maintained unchanged, independently of the filler amount, in the HNT-SA nanocomposites. These two different trends were also observed in nanocomposites of HDPE with dendritic silica (DS) prepared using identical polymerization routes [23]. This point seems to indicate the key role that method for incorporation of filler plays in the resultant size of HDPE crystallites, independently of the type of filler added, in terms of either particle size or aspect ratio (nanometric spheres of for DS and tubes for HNT with length in the axial direction of above 200 nm).

Variation of the degree of crystallinity (f_c^{F1}) with the HNT content (normalized to the actual polymer content in the composite) shows two distinct behaviors, which depend also on the synthetic protocol. In the HNT-MAO set of nanocomposites, crystalline fraction remains almost constant with filler composition and similar to that developed in the pure HDPE. On the contrary, crystallinity increases with increasing HNT content for nanocomposites prepared by the HNT-SA route, as deduced from Table 4.

Results on cooling from the melt, represented in Fig. 5b, are also very
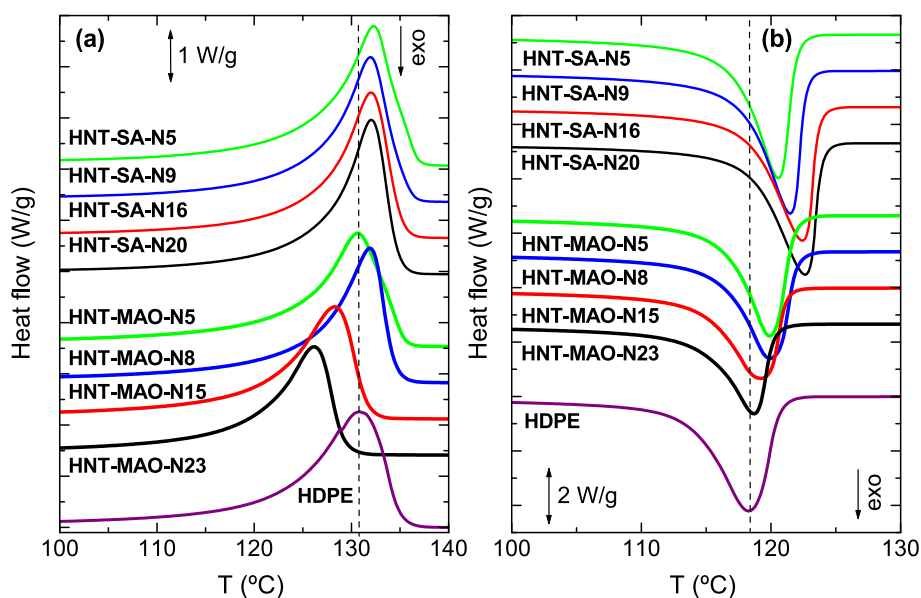
Table 4

HNT content obtained from thermogravimetric analysis (TGA), normalized crystallinity obtained from either WAXD (f_c^{WAXD}) or DSC (f_c^{F1}, f_c^C and f_c^{F2}, for the first melting, cooling and second melting, respectively), as well as melting temperatures from the first (T_m^{F1}) and the second melting (T_m^{F2}) processes, and crystallization temperature (T_C).

Sample	HNT content (wt %)	f_c^{WAXD}	f_c^{F1}	T_m^{F1} (°C)	f_c^C	T_c (°C)	f_c^{F2}	T_m^{F1} (°C)
HDPE	0	0.58	0.56	131.5	0.60	118.0	0.60	132.5
HNT-MAO-N5	5	0.57	0.55	131.0	0.58	120.0	0.58	133.0
HNT-MAO-N8	8	0.57	0.56	134.0	0.59	120.0	0.59	131.5
HNT-MAO-N15	15	0.57	0.56	128.5	0.59	119.0	0.59	129.5
HNT-MAO-N23	23	0.57	0.55	126.0	0.58	118.5	0.59	128.0
HNT-SA-N5	5	0.58	0.58	132.5	0.62	120.5	0.62	134.0
HNT-SA-N9	9	0.58	0.61	132.0	0.64	121.5	0.64	134.0
HNT-SA-N16	16	0.58	0.64	132.0	0.67	122.5	0.68	134.5
HNT-SA-N20	20	0.58	0.65	132.5	0.68	122.5	0.69	134.0

Fig. 5. DSC curves of the HNT based nanocomposites for the first heating (left) and cooling runs (right), at 10 °C/min.

interesting. The common feature, independently of how HNT have been incorporated into HDPE, is the nucleant effect that their presence exerts in the polymeric matrix [44,45]. Thus, crystallization temperature (T_c) is moved to higher temperatures compared with that exhibited by the pristine HDPE. These results are in agreement with several previous investigations that suggested that the inorganic nanofiller particles act as crystallization seeds for the polyolefinic matrix. Du *et al.* [44] described the crystallization behavior of polypropylene and HNT composites, observing that the nanotubes acted as nucleating agents with a behavior similar to that found in silica reinforced nanocomposites. Ning *et al.* [45] also prepared polypropylene and HNT composites via melt processing and found an analogous shift in the crystallization temperature towards higher values with HNT addition, which was also ascribed to a nucleating effect.

An opposite trend is, however, seen for the T_c variation with the HNT amount present in the nanocomposites depending on the synthetic method used. The T_c is shifted to lower temperature as HNT content raises in the HNT-MAO series while its location is moved to higher temperatures with increasing filler composition for the HNT-SA samples. This hindrance observed in the former as HNT is enlarged could be related to the distinct morphological characteristics of the two

composite families, being dispersion of HNT less uniform in the HNT-MAO materials, fact that can alter the nucleation and development of crystallites.

The degree of crystallinity estimated from the cooling and the subsequent second melting run is very similar and shows the same dependencies as observed during the first melting process, although the values are higher. This fact can be ascribed to the slower cooling rate used in the calorimetric experiments (10 °C/min) compared with that applied during the processing by compression molding. A slower cooling rate yields more time for the polymer chains to neatly fold and, as such, results in more and thicker crystallites, larger crystallinity and higher T_m values.

3.2.5. Mechanical behavior

Stress–strain measurements have been performed for evaluation of the mechanical response. This simple but versatile technique provides important information on the characteristics of a material under stress, its stiffness and some other significant parameters. The uniaxial deformation process for the different HNT reinforced nanocomposites and for the pristine HDPE used as reference is depicted in Fig. 6 and the corresponding average values for distinct mechanical magnitudes, deduced
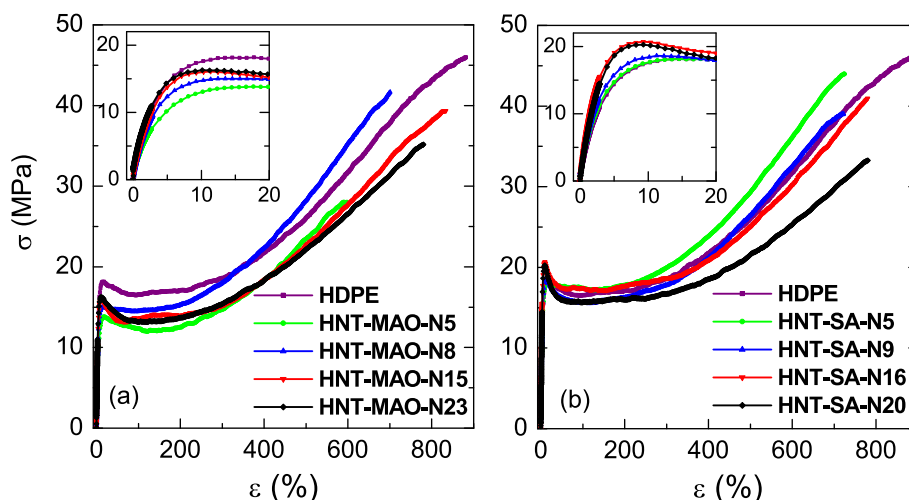

Fig. 6. Stress–strain curves for the HNT-MAO (left) and HNT-SA (right) nanocomposites at room temperature. Pristine HDPE is included as reference.

from the several tests carried out at a given material, are listed in Table 4.

The engineering stress–strain curves observed in Fig. 6 represent the common behavior at room temperature for ductile thermoplastic polymers, such as HDPE, i.e., the so-called cold deformation mechanism. Three regions are evidently distinguishable in each curve: the first one concerning of the initial elastic response, where the stress changes linearly with strain and allows determination of the corresponding elastic Young's modulus (E) value. After this initial stage a yield point is shown, followed by a narrow zone where the stress is maintained relatively unchanged with strain. This yield point enables estimation of the yield stress (σ_Y) of the material, which can be considered as the minimal stress required for inducing a permanent deformation in the material. The last region is marked by the point from which the stress once again starts to rise with strain, due to a chain hardening phenomenon associated with stress-induced orientation of the polymer macrochains. The final phase ends with the break of the material, at which point the corresponding ultimate stress (σ_{break}) and elongation at break (ε_{break}) parameters can be achieved.
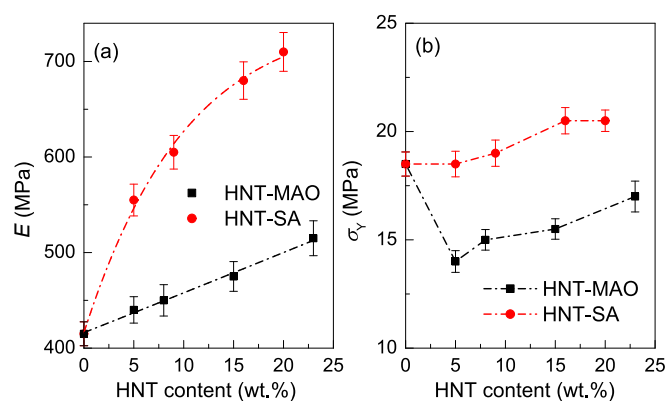
The cold deformation mechanism observed is indicative of necking formation, an occurrence that was simultaneously detected through the *in-situ* observation of the stretching process of the different samples. The existence of a narrow necking propagation stage also indicates that the materials are somewhat soft. Good reproducibility was found in the different materials in relation to the stretching process and parameters deduced from the distinct curves attained in the different strips.

Curves depicted in Fig. 6 show that deformation mechanism is not dependent on polymerization procedure. Nevertheless, some differences can be deduced either from the Fig. 6 or the results listed in Table 5. Concerning the elastic modulus, incorporation of HNT into HDPE, independently of the synthetic protocol, leads to stiffer materials. Thus, an increase in the E values is observed, which are raised as amount of HNT is enlarged in the composite. This feature is ascribed to the reinforcement role that addition of a hard filler plays in the rigidity of the HDPE matrix. The E variation with HNT content is linear in the HNT-MAO family while a more significant improvement in stiffness is noticeable for the HNT-SA hybrids, as clearly deduced from Fig. 7. In fact, the E enlargement when comparing the pristine HDPE with the nanocomposites with the highest HNT composition amounts to 25 % in the former and to 71 % in the latter. Reasons behind this remarkable difference are attributed to the higher crystallinity, the thicker crystallites, the more uniform HNT distribution within HDPE and the better properties in the filler-polymer interfaces found in the HNT-SA

Fig. 7. Dependence of mean values for Young's modulus (E) and yield stress (σ_Y) on HNT clay content for the different HDPE/HNT nanocomposites and the pristine HDPE taken as reference.

nanocomposites. These parameters also affect the values of yielding stress, which are correspondingly larger in HNT-SA materials, as expected from previously observed structural and morphological characteristics.

Concerning parameters at break, all the nanocomposites behave as ductile materials despite the largest HNT content in both families is rather elevated, around 20 wt%. It is expected that the polymers reinforced with inorganic fillers show a significant reduction of their breaking properties at high loadings, since the rigid particles can act as stress concentrators within the matrix. Here, the average elongation at break for all the samples are higher than 600 % and, this is even more relevant in the HNT-SA set of materials since they are considerably stiffer, as deduced from their values of E. This remarkable feature must be associated with their morphological details, since in principle these nanocomposites would be expected to break at much lower deformations due to the characteristics of their crystalline phases. An optimal adhesion at polymer-filler interfaces seems to have been triggered during their synthetic process allowing reaching those excellent parameters at break comparable with those exhibited by the pristine HDPE. This is an unusual feature in nanocomposites based on polyolefins due to the inherent difficulties in achieving a suitable compatibilization between the hydrophilic surface of the filler and the hydrophobic nature of the matrix. The results suggest that, despite both procedures employed in the preparation of the nanocomposites allow obtaining an appropriate compatibilization between the two moieties, the HNT-SA route is much more effective. Indeed, the largest values of σ_{break} and ε_{break} are found in the HNT-SA set of materials. These differences become more outstanding when focus is centered in the binomial Young's modulus—elongation at break. Usually, an increase in E values is accompanied by a decrease of the ε_{break} ones. This feature is not observed when comparing samples HNT-SA-20 and HNT-MAO-N23: the latter exhibits an average ε_{break} of 770 % and a E value of 515 MPa versus an average ε_{break} of 840 % and a E value of 710 MPa for HNT-SA-20. Despite the high amount of filler incorporated and the great improvement in rigidity, the HNT-SA-20 sample behaves as a ductile material similar to pristine HDPE. Thus, the excellent mechanical response observed in the HNT-SA samples should be ascribed to their better morphological characteristics compared with those exhibited by the HNT-MAO hybrids. The remarkably superior HNT distribution and optimal adhesion at polymer-filler interfaces attained in the former makes it possible to counteract in the properties at break the adverse contribution that their higher crystallinity and thicker crystals should impart. These excellent morphological features (in terms of dispersion and phase compatibilization) are also macroscopically noticeable from the aspect of films, which exhibit very good optical characteristics. Values of these magnitudes are those found in compression molded films. Nevertheless, they could be somehow different if materials were

Table 5
Average values for Young's modulus (E), yield stress (σ_Y), ultimate stress (σ_{break}) and elongation at break (ε_{break}) for the different HDPE/HNT nanocomposites and the neat HDPE.

Sample	HNT content (wt %)	E (MPa)	σ_Y (MPa)	σ_{break} (MPa)	ε_{break} (%)
HDPE	0	415 ± 12	18.5 ± 0.4	40 ± 2	840 ± 50
HNT-MAO-N5	5	440 ± 15	14.0 ± 0.5	28 ± 2	600 ± 60
HNT-MAO-N8	8	450 ± 18	15.0 ± 0.5	38 ± 4	740 ± 50
HNT-MAO-N15	15	475 ± 20	15.5 ± 0.6	43 ± 4	930 ± 60
HNT-MAO-N23	23	515 ± 20	17.0 ± 0.7	33 ± 4	770 ± 70
HNT-SA-N5	5	555 ± 20	18.5 ± 0.5	41 ± 1	670 ± 40
HNT-SA-N9	9	605 ± 20	19.0 ± 0.5	44 ± 1	730 ± 40
HNT-SA-N16	16	680 ± 20	20.5 ± 0.8	44 ± 2	910 ± 60
HNT-SA-N20	20	710 ± 25	20.5 ± 0.8	36 ± 3	840 ± 40

processed by extrusion or injection molding. A slightly higher E values would be expected since these two techniques would probably lead to a partial alignment of HNT along axial direction improving rigidity. And, accordingly, somewhat lower deformation at break would be observed.

Comparison of the mechanical properties found in these HNT-SA nanocomposites with those exhibited by the HDPE reinforced with nanoparticles of dendritic silica (DS-SA) prepared by the same methodology [23] indicates that the higher values of E and ε_{break} are achieved in the HNT-SA materials (while the rest of parameters turn out rather similar). In particular, the DS-SA-N21 sample within the DS-SA series is that with the best mechanical performance, exhibiting an E and ε_{break} of 675 MPa and 650 %, respectively [23]. These values are lower than those shown by the HNT-SA-N20 sample, 710 MPa and 840 % as listed in Table 5. This difference can be related to the distinct aspect ratio existing between both reinforcing particles. The long tubes in halloysite provide a superior aspect ratio with respect to that for the spherical dendritic silica. This larger aspect ratio in the HNT may come into play for increasing rigidity as well as during necking propagation and in the strain hardening stage. Alignment of polymer macrochains together with the preferential orientation of the aluminosilicate nanotubes along stretching direction during the cold drawing process may effectively improve ultimate performance for HNT-SA nanocomposites. Nevertheless, the global evaluation of all the materials synthesized seems to point out that mechanical response is controlled more by the crystalline details of the HDPE matrix and by the overall morphological characteristics derived from the synthetic protocol than from the type of filler incorporated. Accordingly, differences in the mechanical parameters are more significant when changing the synthetic route than varying the type of filler.

4. Conclusions

Different nanocomposites based on HDPE and HNT, as reinforcement, were successfully synthesized by *in situ* polymerization using two different approaches, including an innovative route related to the in-situ catalyst supporting concept, recently described for nanocomposites of HDPE and dendritic silica, and a more common procedure for catalyst carrying.

The HNT-SA protocol gave rise to higher polymerization activities and better morphological features, in terms of HNT dispersion and filler-polymer interface properties, when compared with their HNT-MAO counterparts. Moreover, the HNT-SA procedure leads to materials with higher crystallinity, thicker crystals and, consequently, stiffer than those prepared by the HNT-MAO approach, although an increase in rigidity was also observed in the latest. In fact, the improvement in rigidity was above 70 %, when compared with the HDPE reference sample, for HNT-SA-20 and of 25 % for HNT-MAO-23. Furthermore, all the nanocomposites, independently of the preparation method used, exhibited an elongation at break always higher than 600 %, even at amounts of HNT incorporated within HDPE as high as around 20 wt%. Therefore, a remarkable synergy between rigidity and toughness (as well as deformation capacity) is attained in these materials but especially in those obtained by HNT-SA synthetic route. In particular, the HNT-SA-20 sample, which is the one with the best mechanical performance, does show similar ultimate deformation at break compared with that exhibited by the pristine polymeric matrix, despite the strong increase in stiffness (greater than70 %) observed in the nanocomposite.

Summarizing, HNT was revealed to be an interesting and cost-effective filler to be applied in the preparation of high-performance polyethylene nanocomposites. Moreover, comparison of the mechanical properties found in HNT-SA materials with those previously reported for DS-SA ones highlights the beneficial impact of using a high aspect ratio support such as HNT. It is also worth noting that, somewhat unexpectedly, the results here discussed show that polymerization activity, polymer features and derived properties found in the ultimate materials are less impacted by support/filler nature than by preparation method.

This highlights the specificity and distinct features of each approach and confirms the strong potential of the SA route for the preparation of high-performance polyethylene-based nanocomposites with an excellent balance between stiffness and deformability.

Data availability

The raw/processed data required to reproduce these findings cannot be shared at this time due to technical and time limitations.

CRediT authorship contribution statement

Duarte M. Cecílio: Formal analysis, Investigation, Validation, Data curation, Writing – original draft. **Maria L. Cerrada:** Formal analysis, Methodology, Investigation, Funding acquisition, Writing – original draft, Writing – review & editing. **Ernesto Pérez:** Investigation, Funding acquisition, Writing – review & editing. **Auguste Fernandes:** Investigation, Writing – review & editing. **João Paulo Lourenço:** Writing – original draft, Writing – review & editing. **Timothy F.L. McKenna:** Conceptualization, Methodology, Writing – review & editing. **M. Rosário Ribeiro:** Conceptualization, Funding acquisition, Methodology, Project administration, Supervision, Writing – review & editing.

Declaration of Competing Interest

The authors declare that they have no known competing financial interests or personal relationships that could have appeared to influence the work reported in this paper.

Data availability

The raw/processed data required to reproduce these findings cannot be shared at this time due to technical and time limitations.

Appendix A. Supplementary material

Supplementary data to this article can be found online at https://doi.org/10.1016/j.eurpolymj.2022.111765.

References

[1] A. Kubacka, M.L. Cerrada, C. Cerrano, M. Fernández-García, M. Ferrer, M. Fernández-García, Light-Driven Novel Properties of TiO2-Modified Polypropylene-Based Nanocomposite Films, J. Nanosci. Nanotechnol. 8 (2008) 1–6.

[2] J. Arranz-Andrés, E. Pérez, M.L. Cerrada, Hybrids based on poly(vinylidene fluoride) and Cu nanoparticles: Characterization and EMI shielding, Eur. Polym. J. 48 (2012) 1160–1168.

[3] M. Campos, J.P. Lourenço, H. Cramail, M.R. Ribeiro, Nanostructured silica materials in olefin polymerisation: From catalytic behaviour to polymer characteristics , Prog. Polym. Sci., http://doi.org/10.1016/j.progpolymsci.2012.02.006.

[4] W. Ma, Y. Li, M. Zhang, S. Gao, J. Cui, C. Huang, G. Fu, Biomimetic Durable Multifunctional Self-Cleaning Nanofibrous Membrane with Outstanding Oil/Water Separation, Photodegradation of Organic Contaminants, and Antibacterial Performances, ACS Appl. Mater. Interfaces 12 (2020) 34999–35010.

[5] Wang, D. Liu, Q. Li, C. Chen, Z. Chen, P. Song, J. Hao, Y. Li, S. Fakhrhoseini, M. Naebe, X. Wang and W. Lei, Lightweight, Superelastic Yet Thermoconductive

Boron Nitride Nanocomposite Aerogel for Thermal Energy Regulation, ACS Nano, http://doi.org/10.1021/ACSNANO.9B02182.

[6] B.I. Oladapo, S.A. Zahedi, F.T. Omigbodun, A systematic review of polymer composite in biomedical engineering, Eur. Polym. J. 154 (2021), 110534.

[7] M.L. Cerrada, C. Serrano, M. Sánchez-Chaves, M. Fernández-García, A. De Andrés, R.J. Riobóo, F. Fernández-Martín, A. Kubacka, M. Ferrer, M. Fernández-García, Biocidal capability optimization in organic - Inorganic nanocomposites based on titania, Environ. Sci. Technol. 43 (2009) 1630–1634.

[8] M.L. Cerrada, R. Benavente, E. Pérez, Crystalline Structure and Viscoelastic Behavior in Composites of a Metallocenic Ethylene-1-octene Copolymer and Glass Fiber, Macromol. Chem. Phys. 203 (2002) 718–726, https://doi.org/10.1002/1521-3935(20020301)203:4%3C718::AID-MACP718%3E3.0.CO;2-S.

[9] M. Campos, J. Paulo Lourenço, E. Pérez, M.L. Cerrada, M.R. Ribeiro, Self-reinforced hybrid polyethylene/mcm-41 nanocomposites: In-situ polymerisation and effect of MCM-41 content on rigidity, J. Nanosci. Nanotechnol., http://doi.org/10.1166/jnn.2009.1298.

[10] D.M. Laura, H. Keskkula, J.W. Barlow, D.R. Paul, Effect of glass fiber and maleated ethylene–propylene rubber content on tensile and impact properties of Nylon 6, Polymer (Guildf) 41 (2000) 7165–7174.

[11] M.L. Cerrada, A. Bento, E. Pérez, V. Lorenzo, J.P. Lourenço, M.R. Ribeiro, Hybrid materials based on polyethylene and MCM-41 microparticles functionalized with silanes: Catalytic aspects of in situ polymerization, crystalline features and mechanical properties , Microporous Mesoporous Mater. . http://doi.org/10.1016/j.micromeso.2016.06.011.

[12] A. Bento, J.P. Lourenço, A. Fernandes, M.L. Cerrada, M. RosárioRibeiro, Functionalization of Mesoporous MCM-41 (Nano)particles: Preparation Methodologies, Role on Catalytic Features, and Dispersion Within Polyethylene Nanocomposites, ChemCatChem 5 (2013) 966–976.

[13] H. Zou, S. Wu, J. Shen, Polymer/Silica Nanocomposites: Preparation, Characterization, Properties, and Applications, Chem. Rev. 108 (2008) 3893–3957.

[14] S. Kango, S. Kalia, A. Celli, J. Njuguna, Y. Habibi, R. Kumar, Surface modification of inorganic nanoparticles for development of organic–inorganic nanocomposites—A review, Prog. Polym. Sci. 38 (2013) 1232–1261.

[15] S.Y. Fu, X.Q. Feng, B. Lauke, Y.W. Mai, Effects of particle size, particle/matrix interface adhesion and particle loading on mechanical properties of particulate–polymer composites, Compos. Part B Eng. 39 (2008) 933–961.

[16] M.L. Cerrada, E. Pérez, J.P. Lourenço, A. Bento, M.R. Ribeiro, Decorated MCM-41/polyethylene hybrids: Crystalline details and viscoelastic behavior, Polymer (Guildf) 54 (2013) 2611–2620.

[17] W. Kaminsky, A. Funck, K. Wiemann, Nanocomposites by In Situ Polymerization of Olefins with Metallocene Catalysts, Macromol. Symp. 239 (2006) 1–6.

[18] L. Wei, T. Tang, B. Huang, Synthesis and characterization of polyethylene/clay–silica nanocomposites: A montmorillonite/silica-hybrid-supported catalyst and in situ polymerization, J. Polym. Sci. Part A Polym. Chem. 42 (2004) 941–949, https://doi.org/10.1002/pola.11053.

[19] A. Bento, J.P. Lourenço, A. Fernandes, M.R. Ribeiro, J. Arranz-Andrés, V. Lorenzo, M.L. Cerrada, Gas permeability properties of decorated MCM-41/polyethylene hybrids prepared by in-situ polymerization, J. Memb. Sci. 415–416 (2012) 702–711.

[20] M. Liu, Z. Jia, D. Jia, C. Zhou, Recent advance in research on halloysite nanotubes-polymer nanocomposite, Prog. Polym. Sci. 39 (2014) 1498–1525.

[21] M. de F. Vieira Marques, J. L. da Silva Rosa and M. C. V. da Silva, Nanocomposites of polypropylene with halloysite nanotubes employing in situ polymerization, Polym. Bull., 2017, 74, 2447–2464, https://doi.org/10.1007/s00289-016-1848-3.

[22] D.M. Cecílio, A. Fernandes, J.P. Lourenço, T.F.L. McKenna, M.R. Ribeiro, Innovative route for the preparation of high-performance polyolefin materials based on unique dendrimeric silica particles, Polym. Chem. 12 (2021) 4546–4556.

[23] D.M. Cecílio, M.L. Cerrada, E. Pérez, A. Fernandes, J.P. Lourenço, T.F.L. McKenna, M.R. Ribeiro, Unique stiffness-deformability features of dendrimeric silica reinforced HDPE nanocomposites obtained by an innovative route, Microporous Mesoporous Mater. http://doi.org/10.1016/j.micromeso.2021.111619.

[24] C.A. Emeis, Determination of integrated molar extinction coefficients for infrared absorption bands of pyridine adsorbed on solid acid catalysts, J. Catal. 141 (1993) 347–354.

[25] F.A. Quinn, L. Mandelkern, Thermodynamics of Crystallization in High Polymers: Poly-(ethylene)1, J. Am. Chem. Soc. 80 (1958) 3178–3182.

[26] B. Wunderlich, *Macromolecular Physics*, Elsevier, 1st edn., 1980.

[27] D. Mingliang, G. Baochun, J. Demin, Newly emerging applications of halloysite nanotubes: a review, Polym. Int. 59 (2010) 574–582, https://doi.org/10.1002/pi.2754.

[28] M. Thommes, K. Kaneko, A.V. Neimark, J.P. Olivier, F. Rodriguez-Reinoso, J. Rouquerol, K.S.W. Sing, Physisorption of gases, with special reference to the evaluation of surface area and pore size distribution (IUPAC Technical Report), Pure Appl. Chem. 87 (2015) 1051–1069.

[29] B. Bac, N. Dung, L. Khang, K. Hung, N. Lam, D. An, P. Son, T. Anh, D. Chuong, B. Tinh, Distribution and Characteristics of Nanotubular Halloysites in the Thach Khoan Area, Phu Tho, Vietnam, *Minerals* 8 (2018) 290.

[30] A. Kausar, Review on Polymer/Halloysite Nanotube Nanocomposite, Polym. Plast. Technol. Eng. 57 (2018) 548–564.

[31] P. Pasbakhsh, G.J. Churchman, J.L. Keeling, Characterisation of properties of various halloysites relevant to their use as nanotubes and microfibre fillers, Appl. Clay Sci. 74 (2013) 47–57.

[32] D.M. Cecílio, A. Fernandes, J.P. Lourenço, M.R. Ribeiro, Aluminum Containing Dendrimeric Silica Nanoparticles as Promising Metallocene Catalyst Supports for Ethylene Polymerization, ChemCatChem 10 (2018) 3761–3769.

[33] A.Y. Sidorenko, A.V. Kravtsova, A. Aho, I. Heinmaa, K.P. Volcho, N. F. Salakhutdinov, V.E. Agabekov, D. Yu, Acid-modified Halloysite Nanotubes as a Stereoselective Catalyst for Synthesis of 2H-Chromene Derivatives by the Reaction of Isopulegol with Aldehydes, ChemCatChem 10 (2018) 3950–3954.

[34] E.S. Goda, K.R. Yoon, S.H. El-sayed, S.E. Hong, Halloysite nanotubes as smart flame retardant and economic reinforcing materials: A review, Thermochim. Acta 669 (2018) 173–184.

[35] K.-J. Chu, J.B.P. Soares, A. Penlidis, Polymerization mechanism forin situ supported metallocene catalysts, J. Polym. Sci. Part A Polym. Chem. 38 (2000) 462–468, https://doi.org/10.1002/(SICI)1099-0518(20000201)38:3%3C462::AID-POLA10%3E3.0.CO;2-O.

[36] K.-J. Chu, J.B.P. Soares, A. Penlidis, Effect of experimental conditions on ethylene polymerization within-situ-supported metallocene catalyst, J. Polym. Sci. Part A Polym. Chem. 38 (2000) 1803–1810, https://doi.org/10.1002/(SICI)1099-0518(20000515)38:10%3C1803::AID-POLA650%3E3.0.CO;2-X.

[37] M.M. Rueda, M.-C. Auscher, R. Fulchiron, T. Périé, G. Martin, P. Sonntag, P. Cassagnau, Rheology and applications of highly filled polymers: A review of current understanding, Prog. Polym. Sci. 66 (2017) 22–53.

[38] A. Marcilla, A. Gómez-Siurana, D. Berenguer, Study of the influence of the characteristics of different acid solids in the catalytic pyrolysis of different polymers, Appl. Catal. A Gen. 301 (2006) 222–231.

[39] P. Yuan, D. Tan, F. Annabi-Bergaya, Properties and applications of halloysite nanotubes: recent research advances and future prospects, Appl. Clay Sci. 112–113 (2015) 75–93.

[40] D.C. Mcfaddin, K.E. Russell, G. Wu, R.D. Heyding, Characterization of polyethylenes by x-ray diffraction and 13C-NMR: Temperature studies and the nature of the amorphous halo, J. Polym. Sci. Part B Polym. Phys. 31 (1993) 175–183, https://doi.org/10.1002/polb.1993.090310206.

[41] M.L. Cerrada, R. Benavente, E. Pérez, Influence of thermal history on morphology and viscoelastic behavior of ethylene-1-octene copolymers synthesized with metallocene catalysts, J. Mater. Res. 16 (2001) 1103–1111, https://doi.org/10.1557/JMR.2001.0153.

[42] K. Shirayama, S.-I. Kita, H. Watabe, Effects of branching on some properties of ethylene/α-olefin copolymers, Die Makromol. Chemie 151 (1972) 97–120.

[43] C.W. Bunn, The crystal structure of ethylene, Trans. Faraday Soc. 40 (1944) 23–25, https://doi.org/10.1039/TF9444000023.

[44] M. Du, B. Guo, J. Wan, Q. Zou, D. Jia, Effects of halloysite nanotubes on kinetics and activation energy of non-isothermal crystallization of polypropylene, J. Polym. Res. 17 (2009) 109.

[45] N. Ning, Q. Yin, F. Luo, Q. Zhang, R. Du, Q. Fu, Crystallization behavior and mechanical properties of polypropylene/halloysite composites, Polymer (Guildf) 48 (2007) 7374–7384.